Mapping glycoside hydrolase substrate subsites by isothermal titration calorimetry

Gennady Zolotnitsky*†, Uri Cogan*†, Noam Adir†‡, Vered Solomon§, Gil Shoham§, and Yuval Shoham*†¶

Departments of *Biotechnology and Food Engineering and ‡Chemistry and †Institute of Catalysis Science and Technology, Technion-Israel Institute of Technology, Haifa 32000, Israel; and §Department of Inorganic Chemistry and Laboratory for Structural Chemistry and Biology, Hebrew University of Jerusalem, Jerusalem 91904, Israel

Communicated by Arnold L. Demain, Drew University, Madison, NJ, June 21, 2004 (received for review February 3, 2004)

Relating thermodynamic parameters to structural and biochemical data allows a better understanding of substrate binding and its contribution to catalysis. The analysis of the binding of carbohydrates to proteins or enzymes is a special challenge because of the multiple interactions and forces involved. Isothermal titration calorimetry (ITC) provides a direct measure of binding enthalpy (ΔH_a) and allows the determination of the binding constant (free energy), entropy, and stoichiometry. In this study, we used ITC to elucidate the binding thermodynamics of xylosaccharides for two xylanases of family 10 isolated from *Geobacillus stearothermophilus* T-6. The change in the heat capacity of binding ($\Delta C_p = \Delta H/\Delta T$) for xylosaccharides differing in one sugar unit was determined by using ITC measurements at different temperatures. Because hydrophobic stacking interactions are associated with negative ΔC_p, the data allow us to predict the substrate binding preference in the binding subsites based on the crystal structure of the enzyme. The proposed positional binding preference was consistent with mutants lacking aromatic binding residues at different subsites and was also supported by tryptophan fluorescence analysis.

Enzymes exhibit an exceptional catalytic power with an acceleration rate (k_{cat}/k_{uncat}) that can exceed 10^{17} (1, 2). Such powerful catalytic action originates, among other things, from the exquisite positional binding of substrates in which the catalytic residues stabilize the charges formed during the transition state (3). In addition, the substrate may be distorted in the binding pocket into a configuration that resembles the transition state. Revealing the fine details of substrate binding, especially the geometry and energetics involved, is essential for understanding the catalytic efficiency of enzymes. Despite the wide diversity in the tertiary structures and binding-site topologies of enzymes, certain common basic features are typically involved in substrate–enzyme interactions. These interactions are reversible, noncovalent, and relatively weak, thus providing enough stability for catalysis, but are also sufficiently low to allow rapid ligand dissociation (1).

Although high-resolution crystal structures of enzyme–substrate complexes provide invaluable insight into the different elements involved in substrate binding, they cannot provide complete information concerning the forces that drive the binding process. In many high-resolution crystal structures, the substrate is held in position by several specific hydrogen bonds. However, the exact contribution of these bonds to binding and/or catalysis often remains obscure. This situation is especially true for cases of relatively weak binding as relevant for most of the enzyme–substrate interactions. Thus, the actual free energy of such binding is typically in the order of $\Delta G = -10$ kcal/mol (K_d in the micromolar range) that can theoretically be satisfied by only about two hydrogen bonds out of the many potential bonds that are usually available. Moreover, the contribution of entropy to binding cannot be easily calculated or determined based on the crystal structure alone. Hence, our understanding of substrate binding and catalysis is significantly improved by exact thermodynamic parameters and their correlation to the corresponding structural and biochemical data. In this regard, thermodynamic measurements are especially valuable in determining the particular driving forces involved in substrate binding and catalysis. The deeper understanding of these enzymatic key parameters can be then used for a rational design of new functionalities.

Isothermal titration calorimetry (ITC) provides a direct measure of binding enthalpy, ΔH_a, allowing the simultaneous determination of the binding parameters, K_a, ΔS_a, ΔG_a, and the binding stoichiometry (4). When the enthalpy of binding is determined at different temperatures, the change in heat capacity ($\Delta C_p = \Delta H_a/\Delta T$) for the binding reaction can be extracted. Negative ΔC_p values were shown in many systems to be associated with hydrophobic stacking interactions, presumably resulting from the dehydration of highly ordered water molecules surrounding the hydrophobic surfaces (5–8). It should be noted, however, that negative ΔC_p can also be obtained in situations where there is cooperative disorder of hydrogen-bonding networks, with no obvious hydrophobic elements, as pointed out by Cooper (9).

Hydrogen bonding and stacking interactions are the dominant interactions in protein–carbohydrate complexes (10, 11). The sugar-hydroxyl groups can serve simultaneously as hydrogen donors and acceptors and may potentially be involved in as many as three hydrogen bonds (as a donor of one hydrogen bond and an acceptor of two) (10). Stacking or hydrophobic interactions of one or both sides of the sugar ring can be formed with aromatic residues at the binding site of the enzyme (10, 12). In this regard, if the sugar ring and the aromatic residue are coplanar, the π electrons of the aromatic residue can form a number of CH–π interactions with the sugar ring (13). It is evident that determining the exact contribution of the various interactions and forces involved in carbohydrate protein binding is a complicated task (10, 11).

Glycoside hydrolases hydrolyze one of the most stable bonds in nature, with half-lives of millions years (2, 14). To date, the amino acid sequences of more than 12,600 glycosidases have been identified, and the sequenced-based classification of their catalytic domains into families and clans is available on the continuously updated Carbohydrate-Active Enzymes (CAZy) server (http://afmb.cnrs-mrs.fr/CAZY). Glycoside hydrolases are the subject of intensive research because of their pivotal role in many fundamental biological processes as well as in a wide range of industrial applications (15, 16). Xylanases (EC 3.2.1.8) hydrolyze the β-1-4 xylose backbone of xylan, the most abundant hemicellulose polymer (17, 18), and are found mainly in glycoside hydrolase families 10 and 11 (19, 20).

Abbreviations: ITC, isothermal titration calorimetry; IXT6, intracellular xylanase from *Geobacillus stearothermophilus* T-6; XT6, extracellular xylanase from *G. stearothermophilus* T-6; X_2, xylobiose; X_3, xylotriose; X_4, xylotetraose; X_5, xylopentaose; X_6, xylohexaose.

Data deposition: The atomic coordinates and structure factors have been deposited in the Protein Data Bank, www.pdb.org (PDB ID codes 1R85 and 1R87).

¶To whom correspondence should be addressed. E-mail: yshoham@tx.technion.ac.il.

In the present study, ITC was used to measure the binding thermodynamics of selected xylosaccharides to two family 10 xylanases from *Geobacillus stearothermophilus* T-6. These ITC measurements provide valuable information concerning the enzyme–substrate interactions and the number of sugar binding sites that are directly involved in each of these enzymes. We also demonstrate herein that the ΔC_p of binding can be correlated with the potential stacking interactions at the different subsites as predicted from the crystal structures. Such an approach can be used as a general tool for determining the preference of binding at specific subsites.

Experimental Procedures

Site-Directed Mutagenesis. Site-directed mutagenesis was performed on the xylanase genes *xynA* (XT6) and *xynA2* (IXT6) (GenBank accession nos. AAC98140 and AAC98123, respectively) from *G. stearothermophilus* T-6 by using the QuikChange site-directed mutagenesis kit (Stratagene). The mutagenic primers for the mutations were as follows (the mutated nucleotides are in bold type): E159Q, 5′-GGGACGTTGT**C**AAT**C**AGGTTGTGGG-3′ and 5′-CCCACAACCT**G**ATT**G**ACAACGTCCC-3′; Y203A, 5′-GCTTTACATGAATGAT**GC**CAATACAGAAGTCG-3′ and 5′-GCACTTCTGTATTG**GC**ATCATTCATGTAAAGC-3′; W273A, 5′-GATGTGAGCATGTAT**GGT****GCA**CCGCCGCGCGCTTAC-3′ and 5′-GTAAGCGCGGCGGCGG**TGC**ACC**A**TACATGCTCACATC-3′; and E134Q, 5′-GGATGTCAT**T**AAT**C**AAGCGGTAGCCGACGAAGG-3′ and 5′-CCTTCGTCGGCTACCGCTT**GA**TT**A**ATGACATCC-3′. All of the mutated genes were sequenced to confirm that only the desired mutations were inserted.

Protein Production and Purification. All enzymes were overexpressed by using the T-7 expression system in *Escherichia coli* strain BL21(DE3) and purified as reported in ref. 21.

Microcalorimetry Titration Studies. Titration calorimetry measurements were performed with a VP-ITC calorimeter (Microcal, Northampton, MA) as described by Wiseman *et al.* in ref. 4. Protein solutions for ITC were dialyzed extensively overnight against buffer A (50 mM Tris·HCl, pH 7.0/100 mM NaCl/0.02% NaN_3). Ligand solutions of birch wood and beech wood xylans (Sigma) and xylobiose (X_2), xylotriose (X_3), xylotetraose (X_4), xylopentaose (X_5), and xylohexaose (X_6) (Megazyme, Wicklow, Ireland) were prepared by diluting with the buffer used for the protein dialysis. Aliquots (10 μl) of the ligand solution at 8.5–20× the binding-site concentration were added by means of a 250-μl rotating stirrer-syringe to the reaction cell, containing 1.41 ml of the 0.1–0.2 mM protein solution. The heat of dilution was determined to be negligible in separate titrations of the ligand into the buffer solution. Calorimetric data analysis was carried out with ORIGIN 5.0 software (MicroCal). Binding parameters such as the number of binding sites (n), the binding constant (K_a, M^{-1}), and the binding enthalpy (ΔH_a, kcal/mol of bound ligand) were determined by fitting the experimental

Table 1. Thermodynamic parameters for xylosaccharide and xylan binding to XT6(E159Q)

Ligand	T, °C	$K_a \times 10^4$, M^{-1}	K_d ($1/K_a$), μM	ΔH_a, kcal/mol	$T\Delta S_a$, kcal/mol	ΔG_a, kcal/mol	ΔC_p, cal/mol·K
Xylosaccharides							
X_2	20	4.1 ± 0.1	24	−6.8 ± 0.1	−0.6	−6.2	
	30	2.6 ± 0.3	38	−6.7 ± 0.5	−0.6	−6.1	−2 ± 5
	40	1.2 ± 0.1	83	−6.9 ± 0.3	−1.1	−5.8	
	50	2.5 ± 0.3	40	−6.8 ± 0.2	−0.6	−6.2	
X_3	20	12 ± 0.5	8.3	−9.0 ± 0.1	−2.2	−6.8	
	30	11 ± 2	9.4	−10.5 ± 0.1	−3.5	−7.0	−94 ± 19
	40	4.9 ± 0.2	20	−10.9 ± 0.1	−4.2	−6.7	
	50	2.9 ± 0.7	34	−12.0 ± 0.2	−5.1	−6.9	
X_4	20	50 ± 2.3	2.0	−13.4 ± 0.1	−5.8	−7.6	
	30	29 ± 5	3.5	−14.4 ± 0.3	−6.8	−7.6	−233 ± 24
	35	17 ± 1.7	5.9	−15.6 ± 0.3	−8.2	−7.4	
	40	15 ± 1.7	6.7	−17.9 ± 0.3	−10.4	−7.5	
	50	8.5 ± 0.6	12	−20.0 ± 1.2	−12.7	−7.3	
X_5	20	280 ± 27	0.36	−13.2 ± 0.1	−4.6	−8.6	
	30	110 ± 14	0.93	−13.6 ± 1.0	−5.3	−8.3	−257 ± 27
	40	84 ± 5	1.2	−16.8 ± 0.1	−8.3	−8.5	
	50	41 ± 2.4	2.4	−21.1 ± 0.2	−12.8	−8.3	
X_6	20	760 ± 100	0.13	−12.8 ± 0.1	−3.6	−9.2	
	30	290 ± 23	0.35	−15.0 ± 0.2	−6.2	−8.8	−380 ± 35
	40	200 ± 23	0.5	−20.3 ± 0.2	−11.2	−9.1	
	50	140 ± 2.3	0.74	−23.7 ± 0.2	−14.7	−9.0	
Xylans							
Beech wood	20	160 ± 22	0.61	−14.4 ± 0.2	−6.1	−8.3	
	30	110 ± 19	0.89	−15.9 ± 0.9	−7.6	−8.3	−330 ± 32
	40	92 ± 5.8	1.1	−20.3 ± 0.2	−11.8	−8.5	
	50	89 ± 1.6	1.1	−23.2 ± 0.9	−14.4	−8.8	
Birch wood	20	130 ± 16	0.79	−10.0 ± 0.1	−1.8	−8.2	
	30	150 ± 20	0.65	−12.6 ± 1.0	−4.2	−8.4	−360 ± 29
	35	160 ± 17	0.64	−14.4 ± 0.1	−5.6	−8.8	
	40	98 ± 8	1.0	−16.4 ± 0.2	−7.8	−8.6	
	50	130 ± 16	0.75	−20.3 ± 0.2	−11.3	−9.0	

Each set of results is based on the average of three independent measurements. The stoichiometry in all experiments with xylosaccharides was very close to 1 (±0.05). The size of a single ''binding unit'' for xylans was adjusted to fit $n = 1$ and was 17 xylose units for beech and birch wood xylans.

Table 2. Thermodynamic parameters for xylosaccharide and xylan binding to IXT6(E134Q)

Ligand	T, °C	$K_a \times 10^4$, M^{-1}	K_d ($1/K_a$), μM	ΔH_a, kcal/mol	$T\Delta S_a$, kcal/mol	ΔG_a, kcal/mol	ΔC_p, cal/mol K
Xylosaccharides							
X_2	20	2.5 ± 0.2	40	−3.9 ± 0.09	2.0	−5.9	
	30	1.6 ± 0.6	63	−3.2 ± 0.8	2.7	−5.9	−1 ± 14
	40	1.3 ± 0.8	77	−3.6 ± 0.1	2.3	−5.9	
	50	1.6 ± 0.2	63	−3.9 ± 0.2	2.3	−6.2	
X_3	20	5.8 ± 0.3	17	−4.1 ± 0.04	2.3	−6.4	
	30	4.3 ± 0.5	23	−4.8 ± 0.3	1.7	−6.5	−90 ± 14
	40	3.6 ± 0.3	28	−5.6 ± 0.1	0.9	−6.5	
	50	3.3 ± 0.7	30	−6.9 ± 0.2	−0.2	−6.7	
X_4	20	28 ± 1.2	3.6	−5.7 ± 0.02	1.6	−7.3	
	30	20 ± 0.2	5.0	−8.2 ± 0.3	−0.8	−7.4	−253 ± 18
	40	11 ± 0.3	9.1	−10.4 ± 0.05	−3.2	−7.2	
	50	7.5 ± 0.4	13	−13.4 ± 0.1	−6.2	−7.2	
X_5	20	78 ± 7.6	1.3	−6.7 ± 0.06	−1.2	−7.9	
	30	47 ± 5	2.1	−7.9 ± 0.1	0.0	−7.9	−242 ± 28
	40	30 ± 1.8	3.3	−11.5 ± 0.1	−3.6	−7.9	
	50	19 ± 0.7	5.3	−13.6 ± 0.06	−5.8	−7.8	
X_6	20	112 ± 10	0.89	−6.4 ± 0.04	−1.8	−8.2	
	30	49 ± 5.8	2.0	−7.4 ± 0.1	0.5	−7.9	−244 ± 34
	40	39 ± 3.5	2.6	−11.4 ± 0.1	−3.4	−8.0	
	50	17 ± 0.5	5.9	−13.2 ± 0.07	−5.4	−7.8	
Xylans							
Beech wood	30	42 ± 2.7	2.4	−6.2 ± 0.04	1.5	−7.9	
Birch wood	30	42 ± 4.2	2.4	−4.7 ± 0.03	3.1	−7.8	

binding isotherms. K_a was primarily determined by the slope of the isotherm in the equivalence point (22). The unknown molar concentration of binding sites of the high-molecular-weight polysaccharides (xylans) was estimated by altering the concentration of ligand (in the calculation), so as to fit one binding site.

Fluorescence Analysis. Fluorescence measurements were performed with a PerkinElmer luminescence LS50B spectrometer at 25°C with excitation and emission wavelengths of 295 and 345 nm (5-nm slit), respectively. After each ligand addition, the mixture was mixed for 3–5 min to allow the system to reach equilibrium. The binding constants were determined by nonlinear least-squares fit of the data to a one-site binding model by using the program GRAFIT 5.0 (23).

Results and Discussion

Thermodynamics of Substrate Binding. The aim of this study was to characterize the binding thermodynamics of xylooligosaccharides and xylans to family 10 xylanases by using ITC. Two xylanases from *G. stearothermophilus* T-6 were used, a 43,808-Da extracellular xylanase, XT6, and a 38,639-Da intracellular xylanase, IXT6. The 3D structures of both enzymes were recently determined by x-ray crystallography (XT6, PDB ID code 1HIZ (24); IXT6, PDB ID code 1N82). Both proteins are made of a single TIM barrel catalytic domain and share ≈40% sequence identity. For the ITC measurements, we used inactive mutants [XT6(E159Q) and IXT6(E134Q)], lacking the catalytic acid base residues to prevent significant hydrolysis of the substrate during the titration experiments.

Table 1 and Table 2 summarize the thermodynamic parameters and the binding constants extracted from the binding isotherms. These parameters are given for both enzymes at a temperature range of 20–50°C. All of the binding interactions were exothermic, and the enthalpy values ranged from −3.2 to −23.7 kcal/mol. For XT6, entropy values were negative and for IXT6, entropy values ranged from $T\Delta S_a = -6.2$ to +2.7 kcal/mol. All of the titration curves fit very well into a single binding model with a calculated n (stoichiometry) of 1 ± 0.05. For both enzymes, the association constants (K_a) for the different xylosaccharides ranged from $\approx 10^4$ M^{-1} for the hydrolytic product X_2 to 10^6 M^{-1} for the substrates X_6 and xylans. These values reflect the different affinities of the substrates and products to the binding site of the enzyme and are well within the range of typical enzyme–substrate binding constants, corresponding to K_d ($\approx K_m$ in most cases) in the range of 0.4 to 40 μM (1). For XT6, the maximum K_a values were with X_6 and xylans, suggesting a binding site of six sugar subsites in this enzyme. For IXT6, similar K_a values were obtained for X_5, X_6, and xylans suggesting a binding pocket of five subsites. Elongated binding sites are relatively common for glycoside hydrolases, as many of them that act on high-molecular-weight polysaccharides have evolved extended binding pockets that accommodate several sugar units. These binding subsites are labeled, according to convention, from $-n$ to $+n$, with $-n$ at the nonreducing end and $+n$ at the reducing end, whereas the cleavage occurs between the −1 and +1 subsites (25).

At 30°C, the free energy of binding of X_2 was −6.1 kcal/mol, and each additional sugar unit resulted in an average free-energy gain (relative to X_2) of about −0.7 kcal/mol (Fig. 1). These results, together with the one-to-one stoichiometry obtained for X_2, strongly suggest that X_2 has high preference to a invariable site and probably also controls the binding preference of longer xylosaccharides.

Binding Preference of Xylosaccharides in the Active Site of XT6. From the thermodynamic parameters obtained at different temperatures, the heat capacity change ($\Delta C_p = \delta \Delta H_a / \delta T$) for the binding reaction could be extracted. Plotting ΔH_a of binding vs. temperature for the various xylosaccharides gave a linear correlation, indicating that ΔC_p for binding is constant at the temperature range used (Fig. 2). The change in heat capacity (ΔC_p) for the interactions of XT6 with different xylosaccharides becomes more negative as the size of the substrate increases (Table 1). The ΔC_p for X_2 is negligible, that for X_3 is −94 cal/mol·K, and those for X_4 and X_5 are about −245 cal/mol·K, and those for X_6 and xylans are about −360 cal/mol·K (Table 1).

BIOCHEMISTRY

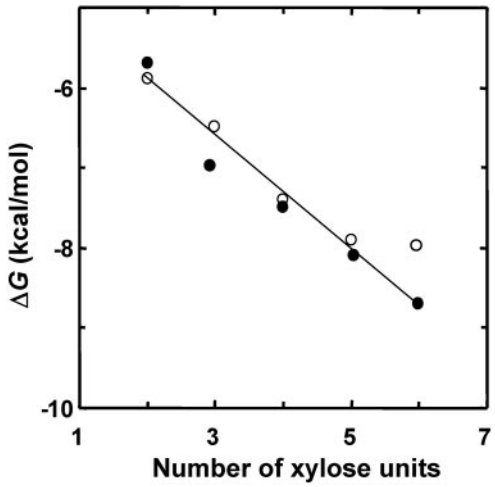

Fig. 1. Free energy of xylosaccharide binding to XT6(E159Q) (●) and to IXT6(E134Q) (○) vs. the number of xylose units in the saccharide chain. Note that for IXT6, X_6 and X_5 give similar values, indicating that in IXT6 there are only five binding subsites.

How do the measured ΔC_p values match the 3D structure of the relevant complexes? Such a correlation can be made on the basis of several crystal structures of enzyme–substrate complexes of XT6, which were recently analyzed. In the crystal structures of XT6 (PDB ID codes 1HIZ in ref. 24 and 1R85) and its complex with its products, cleaved X_5 (PDB ID code 1R87), it is evident that X_3 and X_2 occupy subsites -3 to -1 and $+1$ to $+2$, respectively (Fig. 3). These structures indicate that there are five conserved aromatic residues in the vicinity of the active site that potentially can be involved in stacking interactions with the bound sugars at the different subsites: Trp-316 at subsite -2, Trp-324 at -1, Tyr-203 at $+1$, Trp-273 at $+2$, and Trp-241 at $+3$. A close examination of these residues reveals that in the -2 and -1 subsites, the sugar rings and the aromatic residues have small contact surface area (10–20 Å^2) and are not parallel to each other, a geometry that does not support stacking interactions (Fig. 3*B*). On the other hand, the aromatic residues at the $+1$ and $+2$ subsites are oriented parallel to the sugar rings with a much larger contact surface area (>50 Å^2), making stacking interactions much more favorable (Fig. 3*B*). These overall arrangements of aromatic residues (lacking apparently stacking interactions in subsites -2 to -1 and with stacking interaction in subsite $+1$) are found also in many other family 10 xylanases, for which the structures of xylosaccharide–enzyme complexes are available. These structures include the xylanases from *Cellulomonas fimi* (PDB ID codes 1FH7–1FH10), *Cellvibrio japonicus* (PDB ID code 1E5N), *Penicillium simplicissimum* (PDB ID codes 1B3Y and 1B3Z), *Streptomyces lividans* (PDB ID codes 1EOX and 1EOY), *Streptomyces olivaceoviridis* E86 (PDB ID codes 1ISW and 1ISX), and *Thermoascus aurantiacus* (PDB ID codes 1GOQ and 1GOR) (26–32). Interestingly, a recent struc-

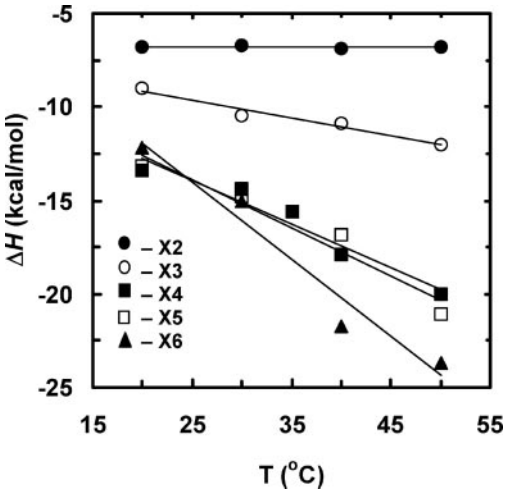

Fig. 2. Changes in the binding enthalpies (ΔH_a) at different temperatures for interaction of xylosaccharides with XT6(E159Q). Values of ΔC_p were derived from the slopes of the linear correlation.

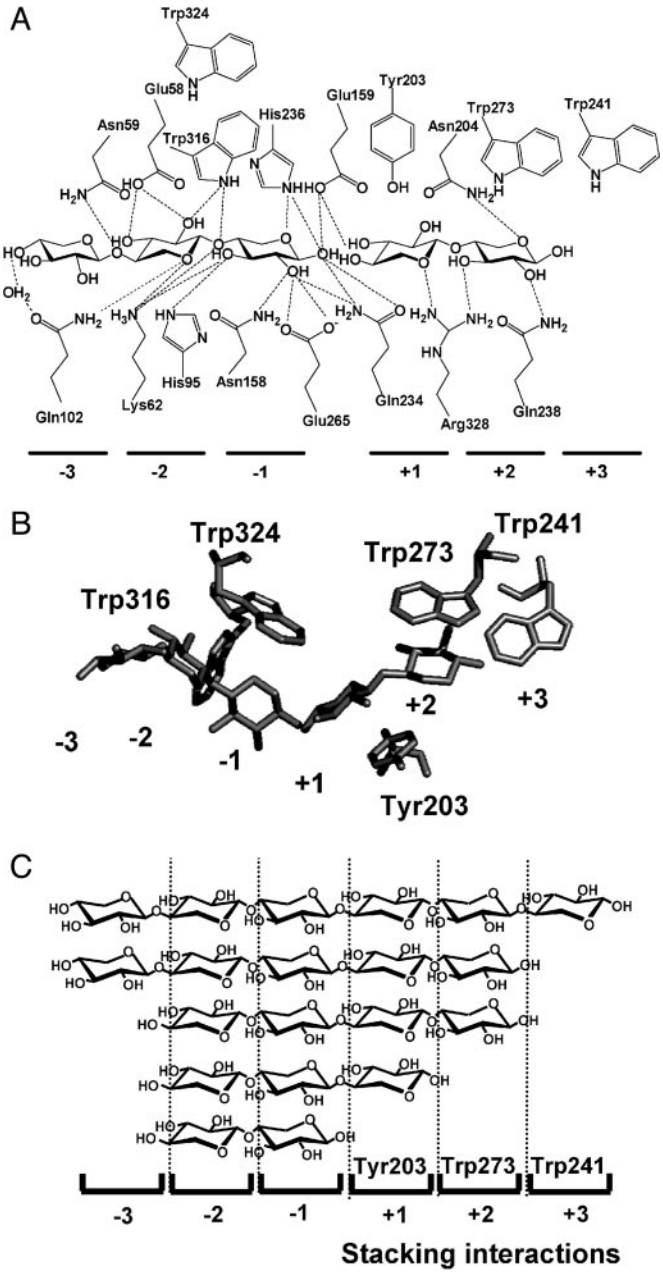

Fig. 3. Substrate positional binding in XT6. (*A*) Schematic representation of the hydrogen bonding network and stacking interactions in the XT6 binding site. (*B*) Structure of XT6 in complex with X_3 and X_2 (cleaved X_5), showing only the aromatic amino acids and the sugars. Tyr-203 and Trp-273 form stacking interactions with the sugar rings at subsites $+1$ and $+2$, respectively. (*C*) The suggested positional binding of xylosaccharides to the binding subsites of XT6, obtained by combining the ΔC_p with the structural data.

Table 3. ΔC_p of binding for different xylosaccharides with mutants lacking binding residues

Enzyme (mutant)	ΔC_p, cal/mol·K								
						Xylan		Stacking	
	X_2	X_3	X_4	X_5	X_6	Birch wood	Beech wood	in subsites	K_a (X_6),* $M^{-1} \times 10^4$
XT6(E159Q)	−2	−94	−233	−257	−380	−330	−360	+1, +2, +3	290
XT6(E159QY203A)	6	−13	−154	−141	−238			+2, +3	19
XT6(E159QW273A)	0	−85	−93	−89	−190			+1, +3	54
IXT6(E134Q)	−1	−90	−253	−242	−244			+1, +2	49
XT6(E159QQ102A)	−5	−118	−239	−267	−359			+1, +2, +3	38

*K_a is for X_6 at 30°C; values are from Tables 1 and 2.

ture of *Cellvibrio japonicus* xylanase in its complex with X_4 (PDB ID code 1US2) indicates a potential stacking interaction at the −3 subsite (33). Taking together the ΔC_p values and the 3D structure of XT6, we can now predict the binding preference of XT6 toward xylosaccharides. The ΔC_p for X_2 was negligible, thus, it is most likely that X_2 binds to the −2 and −1 subsites, where there are no stacking interactions (Fig. 3*C*). X_3 has one stacking interaction and probably occupies the three subsites between −2 and +1 (a single stacking interaction with Tyr-203 at the +1 subsite). X_4 and X_5 seem to have two stacking interactions, and presumably their binding occurs at the −2 to +2 and the −3 to +2 subsites, respectively. Finally, X_6 has three stacking interactions and, therefore, should occupy the six subsites between −3 and +3 (Table 1 and Fig. 3). The same arguments hold for the longer substrate xylan, which should also be bound by three stacking interactions. Based on this assignment, each aromatic residue contributes to ΔC_p about −100 to −150 cal/mol·K. These results are consistent with theoretical and experimental data (34) and also correlate well with values obtained with the xylan binding module CBM15, where two Trp residues are proposed to mediate the main hydrophobic–stacking interactions with X_5, providing ΔC_p of about −300 cal/mol·K (35).

The proposed binding preferences can be challenged by using mutants lacking either the aromatic residues at subsites +1 (Tyr-203) and +2 (Trp-273) or a nonaromatic binding residue, Gln-102 for example. The ΔC_p values of the mutants in the aromatic residues were predicted to be less negative by ≈100–150 cal/mol·K, but only for xylosaccharides that occupy these subsites. For the Gln-102 replacement, ΔC_p should not change (although the K_a may be reduced). Indeed, the ΔC_p values of the mutants were exactly as predicted from the preference of binding suggested above (Fig. 3 and Table 3) with an average ΔC_p loss of −105 to −165 cal/mol·K for Y203A and W273A, respectively, and no ΔC_p change for Q102A (Table 3). It should be noted that although all of the mutations resulted in reduced K_a, the corresponding ΔC_p values support the assigned binding preference.

The positional binding scheme deduced from the thermodynamic data of the extracellular xylanase XT6 is also consistent with the results obtained with the intracellular xylanase IXT6. Both the ITC data (Table 2 and Fig. 1) and the crystal structure of IXT6 (PDB ID code 1N82) suggest that the active site of the enzyme consists of five binding subsites compared with the six subsites of XT6. In the + subsites there are two conserved aromatic residues, Tyr-179 at subsite +1 and Phe-249 at subsite +2 (this enzyme lacks an aromatic residue at position +3). Based on the overall arrangements of enzyme–substrate interactions in the active site of family 10 (no stacking interactions at the minus sites), it is expected that the maximum ΔC_p value with this enzyme will reflect a contribution of two stacking interactions. Indeed, the ΔC_p values observed for X_4, X_5, and X_6 were all similar, about −250 cal/mol·K (Table 3).

Trp Fluorescence Quenching Analysis Supports the Substrate Binding Preference Indicated by ITC. Because several Trp residues are part of the binding subsites, it is possible to use Trp fluorescence quenching analysis to independently determine the xylosaccharides binding mode for this enzyme. XT6 contains 10 Trp residues, 3 of which are likely to interact with the substrate. Trp-316 at the −2 subsite forms hydrogen bonds (but no stacking interaction), and Trp-273 and Trp-241 form stacking interactions at the +2 and +3 subsites, respectively. In the presence of a molar excess of X_6, significant quenching (≈15%) in Trp fluorescence (excitation 295 nm and emission 345 nm) was obtained (data not shown). Titration with various xylosaccharides resulted in quenching curves that are consistent with the binding preference predicted from the ITC analysis (Fig. 4*A*). Thus, X_2 and X_3 resulted in quenching of ≈5%, reflecting the

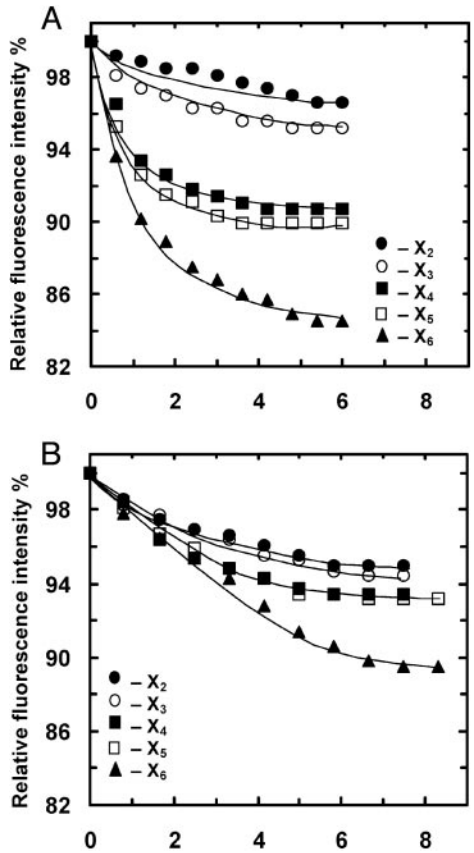

Fig. 4. Changes in fluorescence intensities in the presence of different concentrations of xylosaccharides at 25°C. (*A*) Binding of xylosaccharides to XT6(E159Q). (*B*) Binding of xylosaccharides to XT6(E159QW273A) (lacking Trp-273 at the +2 subsite).

interaction with a single Trp residue (probably Trp-316 at −2). X_4 and X_5 provided additional quenching of up to a total of 10%, suggesting that for both substrates an additional Trp interaction is involved (probably Trp-273 at +2). Finally, X_6 resulted in 15% quenching, indicating interaction with a third Trp residue (probably Trp-241, at +3). The results with the W273A mutant are also consistent with the binding assignment. This mutant lacks the Trp residue at the +2 subsite. Thus, it is expected that the degree of quenching will be similar with X_2, X_3, X_4, and X_5 that interact only with Trp-316 at the −2 subsite. X_6, however, is expected to interact also with Trp-241 at the +3 subsite, thus providing an additional quenching of 5%. As shown in Fig. 4*B*, these expectations are exactly the results obtained. In addition, the Trp quenching titration experiments allow us to determine the xylosaccharide binding constants (K_a). For X_5 and X_6 at 25°C, the K_a values were 99×10^4 and 200×10^4 M^{-1}, respectively, well within the range obtained by the ITC analysis. Taking these results together, the Trp fluorescence quenching analysis provided an additional independent confirmation of the substrate binding preference suggested by the ITC analysis.

Enthalpy–Entropy Compensation Effect. When ΔH_a and $T\Delta S_a$ values for the binding of different xylosaccharides are plotted against each other, a linear relationship is observed with a slope of 1.3 (Fig. 5). Thus, a change in enthalpy is compensated by an opposite change in entropy. This phenomenon, termed enthalpy–entropy compensation, has been described in many systems (36–38), however, the biological relevance of this phenomenon is a matter of debate (39–41). The seemingly linear relationship results, in fact, from the limited range of ΔG_a (K_a values) used in the experiments and the Gibbs free energy relationship, $\Delta G_a = \Delta H_a - T\Delta S_a$ (see dashed lines in Fig. 5). In experiments where the binding constants do not vary significantly (i.e., by more than three orders of magnitude), the ΔH_a to $T\Delta S_a$ relationship must fall within a limited range (within the dashed lines in Fig. 5). However, with both enzymes the binding of X_2, X_3, and X_4 follows a similar trend in which each additional sugar contributes about the same to ΔH_a and ΔS_a. Thus, the binding mechanism of these sugars is likely to be similar. This trend does not follow for X_5, X_6, and xylans, which may indicate that somewhat different binding forces are involved. A mechanistic clue for this phenomenon can be derived from the crystal structures of the enzyme–substrate complexes in which the sugar rings at subsites −2 to +2 are held by a larger number of potential hydrogen bonds.

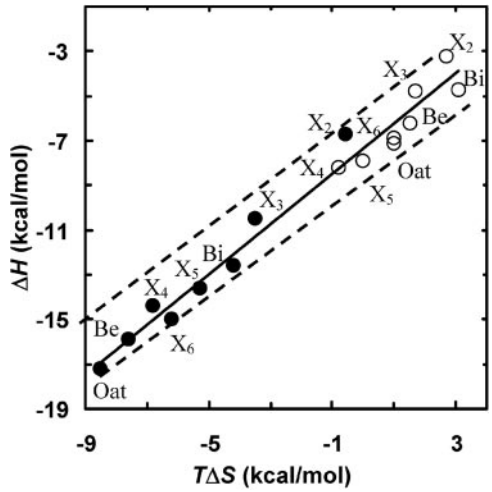

Fig. 5. Enthalpy–entropy compensation plot for the binding of X_2, X_3, X_4, X_5, X_6, beech wood xylan (Be), birch wood xylan (Bi), and oat spelts xylan (Oat) to IXT6 (○) and to XT6 (●) at 303 K. The dashed lines are the theoretical range of ΔG_a, where the binding constants vary by three orders of magnitude.

Conclusions. This study demonstrates that ΔC_p values can be used as a reliable and accurate tool to evaluate the contribution of stacking–hydrophobic interactions to the binding mechanisms. If structural data are available, it may also provide the binding preference of the substrate where more than one binding alternative exists. Because ITC measures enthalpy directly, there is very little error involved in the ΔC_p values regardless of the binding mechanisms and constants. This approach may be applicable for many other systems in which the binding is characterized with measurable changes in ΔC_p.

This study was supported by the German–Israeli Foundation for Scientific Research and Development (to Y.S. and G.S.), the French–Israeli Association for Scientific and Technological Research (to Y.S.), the Israel Science Foundation (to G.S. and Y.S.), and the Otto Meyerhof Center for Biotechnology, Technion, established by the Minerva Foundation (Munich).

1. Fersht, A. (1999) *Structure and Mechanism in Protein Science: A Guide to Enzyme Catalysis and Protein Folding* (Freeman, New York).
2. Wolfenden, R. & Snider, M. J. (2001) *Acc. Chem. Res.* **34,** 938–945.
3. Jencks, W. P. (1975) *Adv. Enzymol. Relat. Areas Mol. Biol.* **43,** 219–410.
4. Wiseman, T., Williston, S., Brandts, J. F. & Lin, L. N. (1989) *Anal. Biochem.* **179,** 131–137.
5. Livingstone, J. R., Spolar, R. S. & Record, M. T., Jr. (1991) *Biochemistry* **30,** 4273–4244.
6. Lemieux, R. U. (1996) *Acc. Chem. Res.* **29,** 373–380.
7. Spolar, R. S. & Record, M. T., Jr. (1994) *Science* **263,** 777–784.
8. Tomme, P., Creagh, A. L., Kilburn, D. G. & Haynes, C. A. (1996) *Biochemistry* **35,** 13885–13894.
9. Cooper, A. (2000) *Biophys. Chem.* **85,** 25–39.
10. Quiocho, F. A. (1989) *Pure Appl. Chem.* **61,** 1293–1306.
11. Quiocho, F. A., Vyas, N. K. & Spurlino, J. C. (1989) *Trans. Am. Crystallogr. Assoc.* **25,** 23–35.
12. Hu, G., Oguro, A., Li, C., Gershon, P. D. & Quiocho, F. A. (2002) *Biochemistry* **41,** 7677–7687.
13. Nishio, M., Hirota, M. & Umezwa, Y. (1998) *The CH/p Interaction: Evidence, Nature, and Consequences* (Wiley, New York).
14. Shallom, D. & Shoham, Y. (2003) *Curr. Opin. Microbiol.* **6,** 219–228.
15. Mackenzine, L. F., Wong, Q., Warren, R. A. & Withers, S. G. (1998) *J. Am. Chem. Soc.* **120,** 5583–5585.
16. Kulkarni, N., Shendye, A. & Rao, M. (1999) *FEMS Microbiol. Rev.* **23,** 411–456.
17. Hazlewood, G. P. & Gilbert, H. J. (1998) *Prog. Nucleic Acid Res. Mol. Biol.* **61,** 211–241.
18. Sunna, A. & Antranikian, G. (1997) *Crit. Rev. Biotechnol.* **17,** 39–67.
19. Thomson, J. A. (1993) *FEMS Microbiol. Rev.* **104,** 65–82.
20. Davies, G. & Henrissat, B. (1995) *Structure (London)* **3,** 853–859.
21. Bravman, T., Zolotnitsky, G., Shulami, S., Belakhov, V., Solomon, D., Baasov, T., Shoham, G. & Shoham, Y. (2001) *FEBS Lett.* **495,** 39–43.
22. Faergeman, N. J., Sigurskjold, B. W., Kragelund, B. B., Andersen, K. V. & Knudsen, J. (1996) *Biochemistry* **35,** 14118–14126.
23. Leatherbarrow, J. R. (2001) GRAFIT (Erithacus Software, Horley, U.K.), Version 5.0.
24. Teplitsky, A., Mechaly, A., Stojanoff, V., Sainz, G., Golan, G., Feinberg, H., Gilboa, R., Reiland, V., Zolotnitsky, G., Shallom, D., *et al.* (2004) *Acta Crystallogr. D* **60,** 836–848.
25. Davies, G., Wilson, K. S. & Henrissat, B. (1997) *Biochem. J.* **321,** 557–559.
26. White, A., Withers, S. G., Gilces, N. R. & Rose, D. R. (1994) *Biochemistry* **33,** 12546–12552.
27. Dominguez, R., Souchon, H., Spinelli, S., Dauter, Z., Wilson, K. S., Chauvaux, S., Beguin, P. & Alzari, P. M. (1995) *Nat. Struct. Biol.* **2,** 569–576.
28. Derewenda, U., Swenson, L., Green, R., Wei, Y., Morosoli, R., Shareck, F., Kluepfel, D. & Derewenda, Z. S. (1994) *J. Biol. Chem.* **269,** 20811–20814.
29. Harris, G. W., Jenkins, J. A., Connerton, I. & Pickersgill, R. W. (1996) *Acta Crystallogr. D* **52,** 393–401.
30. Schmidt, A., Schlacher, A., Schwab, W. & Kratky, C. (1998) *Protein Sci.* **7,** 2081–2088.
31. Natesh, R., Bhanumoorthy, P., Vithayathil, P. J., Sekar, K., Ramakumar, S. & Viswamitra, M. A. (1999) *J. Mol. Biol.* **288,** 999–1012.
32. Fujimoto, Z., Kuno, A., Kaneko, S., Yoshida, S., Kobayashi, H., Kusakabe, I. & Mizuno, H. (2000) *J. Mol. Biol.* **300,** 575–585.
33. Pell, G., Szabo, L., Charnock, S. J., Xie, H., Gloster, T. M., Davies, G. J. & Gilbert, H. J. (2004) *J. Biol. Chem.* **279,** 11777–11788.
34. Makhatadze, G. I. & Privalov, P. L. (1990) *J. Mol. Biol.* **213,** 375–384.
35. Pell, G., Williamson, M. P., Walters, C., Du, H., Gilbert, H. J. & Bolam, D. N. (2003) *Biochemistry* **42,** 9316–9323.
36. Chervenak, M. C. & Toone, E. J. (1995) *Biochemistry* **34,** 5685–5695.
37. Srimal, S., Surolia, N., Balasubramanian, S. & Surolia, A. (1996) *Biochem. J.* **315,** 679–686.
38. Xie, H., Bolam, D. N., Nagy, T., Szabo, L., Cooper, A., Simpson, P. J., Lakey, J. H., Williamson, M. P. & Gilbert, H. J. (2001) *Biochemistry* **40,** 5700–5707.
39. Cornish-Bowden, A. (2002) *J. Biosci. (Bangalore, India)* **27,** 121–126.
40. Sharp, K. (2001) *Protein Sci.* **10,** 661–667.
41. Cooper, A., Johnson, C. M., Lakey, J. H. & Nollmann, M. (2001) *Biophys. Chem.* **93,** 215–230.